

Synchronicity in Composite Hydrogels: Belousov–Zhabotinsky (BZ) Active Nodes in Gelatin

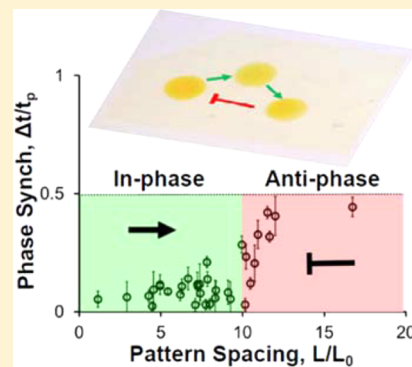
Philip R. Buskohl,^{†,‡} Ryan C. Kramb,^{†,‡} and Richard A. Vaia*,[†]

[†]AFRL/RX Materials & Manufacturing Directorate, Air Force Research Laboratory, Wright-Patterson AFB, Ohio 45433, United States

[‡]UES, Inc., Dayton, Ohio 45432, United States

Supporting Information

ABSTRACT: Synchronization of motion, task, or communication is responsible for the successful function of many living systems. Composite Belousov–Zhabotinsky (BZ) self-oscillating hydrogels exhibit a sufficiently complex chemical-mechanical feedback to develop synchrony and other dynamical behaviors. In the context of BZ gels, synchrony is the sustained, oscillating oxidation with constant phase of two or more catalyst-immobilized gel segments. However, design criteria to control chemical-mechanical synchronization through patterning of the reaction catalyst are lacking. To characterize the fundamental units of composite device design, the periodic oxidation behavior of isolated nodes, node pairs, and multinode systems were investigated. Isolated nodes of Ru-immobilized gelatin exhibited three distinct, volume-dependent, regimes of oscillation: (i) long period (10–40 min), (ii) biperiod (mix of long and short), and (iii) short period (2.5 min). Node pairs and multinode grids of Ru gelatin were embedded in plain gelatin through a film stacking or 3D printing technique. The fraction of synchronized node pairs decreased with increasing interspace distance. Embedment increased the probability of synchronization, with 100% synchronization for interspace distances of less than 10 times the characteristic length of the reaction–diffusion process. The phase difference between synchronized node pairs transitioned from in-phase at small interspace distances to antiphase at large distances, providing the first experimental verification of antiphase synchrony in composite BZ gels. From these design criteria and fabrication techniques, the chemical-mechanical feedback of BZ composites can be programmed through strategic patterning of the catalyst to build BZ devices for sensor, trigger, or chemical computing applications.



1. INTRODUCTION

Self-organization and synchrony are behaviors that are clearly demonstrated in living systems. Fireflies blink in unison to coordinate mating calls, schools of fish swarm to evade and intimidate predators, and slime molds demonstrate advantageous collective behavior.^{1–4} In each example, an assembly of complex, interdependent units develops order through the excitation and feedback of relatively rudimentary signals between near-neighbors (light, motion, chemical). Synchrony exists in synthetic systems as well, such as electrons in an electrochemical potential⁵ and assemblies of chemically oscillating particles,⁶ suggesting that spontaneous organization could be encouraged through appropriate material design. Such materials provide a unique framework in which to perturb the dynamics of synchrony and identify the key parameters to indirectly regulate autonomous networks. Furthermore, material synchrony and logic represent the next step in the evolution of adaptive materials and are critical building blocks for the effective design of sensing and computing materials.

The Belousov–Zhabotinsky (BZ) chemical reaction has the necessary ingredients (excitation and feedback) for synchrony, dynamic self-organization, and even chaotic behavior.⁷ BZ reactions involve a periodic oxidation and reduction of a metal

catalyst in a solution consisting primarily of nitric acid (HNO_3), sodium bromate (NaBrO_3), and malonic acid [MA, $\text{CH}_2(\text{COOH})_2$]. The activator molecule HBrO_2 facilitates the oxidation of the metal catalyst while simultaneously increasing its own supply. Malonic acid, in turn, facilitates the reduction of the metal catalyst while creating bromide ions that inhibit the oxidation process. Immobilizing the catalyst (typically Ru or Fe) in a hydrogel results in an autonomous swelling and deswelling response to changes in the charge state of a catalyst.⁸ The Ru-immobilized polymer, denoted as “active”, fundamentally behaves as an autonomous oscillator when placed in a solution of BZ reactants. Monoliths of active hydrogels have been extensively studied, with particular interest in maximizing the mechanical performance (swelling) of the gel.^{9,10} The effects of monolith shape, aspect ratio, and relative size on the period of oxidation and point of initiation have also been investigated.^{11,12} Furthermore, the bidirectional chemomechanical feedback in monoliths has been demonstrated through mechanical resuscitation of catalyst oxidation oscillations,¹³

Received: December 23, 2014

Revised: February 2, 2015

suggesting that active gels might also communicate mechanically in addition to sensing each other's chemical wake.

Composite BZ hydrogels, which consist of active and inactive regions, provide a platform for studying the mechanical and chemical synchrony between active gel regions and enable the occurrence of oscillation behaviors that are not possible in monolith systems. For the BZ system, synchrony is defined as the sustained, periodic oxidation at constant phase of two or more segments of active BZ gels. Tateyama et al.¹⁴ demonstrated that isolated shapes of Ru-immobilized gel could transmit a unidirectional wave of oxidation when placed within a critical distance from each other. This critical interspace distance was positively correlated with nitric acid concentration, confirming that the chemical communication and diffusion length scales are interconnected. Synchronization behavior has also been shown in Poly N-isopropylacrylamide (PNIPAM) nodes separated by polyacrylamide (PAM) spacers, where the oxidation direction was oriented toward gels of larger size and higher catalyst concentration.¹⁵ The maximum interspace distance for synchronization to occur was reported to be 420 μm , with consistent synchronization for interspace distances of <230 μm . Smith et al.¹⁶ observed a transition in synchrony from near-in-phase synchrony to no synchrony in fully embedded gelatin composites as active nodes were placed farther apart. The gelatin system had the additional benefit of chemical cross-linking at the interfaces between active and plain gelatin regions, which facilitates mechanical coupling.

Computational models of composite BZ gels have predicted the importance of interspace distance in synchrony, including the yet to be experimentally observed transition from in-phase to antiphase synchronization with increasing spacing.¹⁵ The models include a mechanical coupling term that relates to the mechanical communication possible in robustly interconnected regions of active and inactive gel. According to the models, mechanical coupling eliminates oscillation death at small interspace distances, potentially because of a stabilizing effect from embedment.¹⁷ Mechanical coupling was also predicted to increase the frequency of synchronized oxidation oscillations compared to those without embedment (i.e., mechanical coupling).¹⁷ The frequency shift of mechanical coupling has not yet been experimentally demonstrated.

In this study, the fundamental building blocks for BZ composites, namely, isolated single nodes, node pairs, and multinode arrays, were characterized. Two fabrication techniques were developed to make mechanically robust, composite BZ thermogels with precise boundaries between active and inactive regions. Isolated nodes demonstrated three regimes of distinct period behavior that depend on gel volume. Robust criteria for synchrony over a large number of consecutive oscillations (>30) were employed. The computationally predicted transition in phase difference with interspace distance was experimentally verified, and antiphase synchrony was observed for the first time in a composite BZ gel. The results of this study provide a framework for composite BZ device design and bring materials with the capacity for synchrony closer to engineering use.

2. RESULTS AND DISCUSSION

2.1. Composite Fabrication Techniques for BZ Gels.

Composite BZ gels require the assembly of catalyst-immobilized (active) and catalyst-free (inactive) hydrogel regions separated by distinct spatial boundaries. Two techniques, film stacking and three-dimensional (3D) printing,

were utilized in this study to create the composite gels. Using the thermogelation properties of gelatin, the active gelatin in the liquid state was poured into molds to create thin films (0.4–1.0 mm thick) that congealed at room temperature (22–24 °C). Segments of these films were then manually cut, placed in a pattern, and then backfilled with liquid plain gelatin (~46 °C). The elevated temperature of the plain gelatin not only facilitated pouring during backfilling, but promoted mechanical connection to the active gelatin through the entanglement of the chains. For the node-pair specimens, two parallel strips of active gelatin were embedded in a rectangular block of plain gelatin that was then sliced using a custom cutting jig (Figure 1A). Cut specimens were ~0.5 mm thick. Images of the cutting jig and fabrication process are included in Figure S1 (Supporting Information).

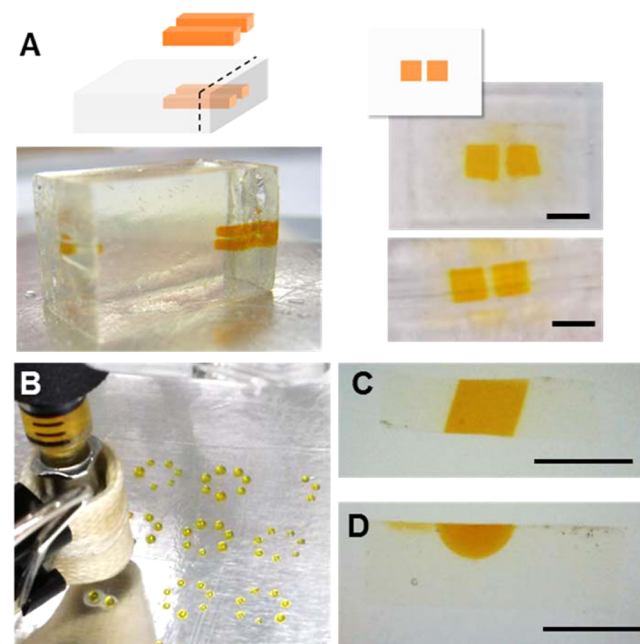


Figure 1. Fabrication techniques for BZ gelatin: (A) Outline of film stacking method where active (orange/yellow) gelatin strips are tiled, embedded, and then cut orthogonally to create square embedded node pairs. Isometric, top, and side views of an embedded node pair. (B) Three-dimensional (3D) printing technique for more complicated patterns. Heat tape maintained the nozzle temperature at 46 °C for optimal viscosity for printing. (C) Profile of film-stacked specimen with active material completely through the thickness. (D) Profile of 3D printed nodes showing embedded hemispherical cap. Scale bars = 1 mm.

More complicated patterns were fabricated using the Fab@Home 3D printing system (Figure 1B). The Fab@Home system consists of a computer-controlled 3D stage and extruder. The gelatin was heated in the extruder to ~46 °C to facilitate extrusion and congealed within 15 s after being printed on a room-temperature (22–24 °C) plate lined with Bytac film. Heated plain gelatin was then backfilled over the printed BZ gel as was done in the film stacking method. Print parameters are included in Table S1 of the Supporting Information. The through-thickness profile of the 3D printed gel differed from that of the film-stacked gels. Film-stacked specimens were patterned completely through the thickness of the embedding matrix and maintained a square shape (Figure 1C), whereas printed nodes formed hemispherical caps that did

not extend entirely through the thickness of the embedding gel (Figure 1D).

2.2. Oscillation Behavior Dependent on Volume. To characterize the fundamental building block of BZ composites, the period behavior of an isolated, Ru-immobilized node was first evaluated. Three distinct regimes of oscillation behavior were observed and showed a dependence on gel volume (Figure 2). At small volumes, only long-period oscillations

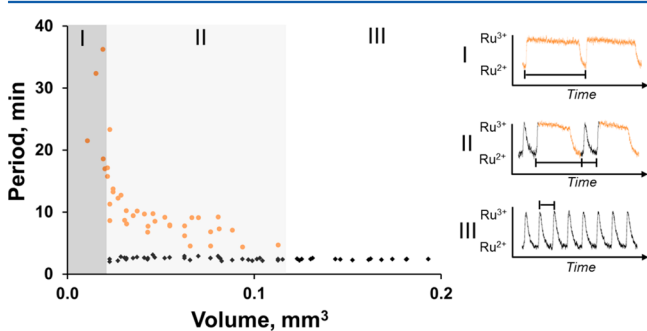


Figure 2. Dependence of period behavior on active-node volume. Three oscillation regimes observed: (I) long periods at small volume (orange), (II) mix of short and long oscillations at intermediate volumes, and (III) short periods only at large volumes greater than 0.1 mm^3 . Side panel: Representative oxidation waveforms and period measurements for each regime.

occurred, with the gel remaining oxidized (Ru^{3+}) for the majority of the oscillation (regime I, dark gray). At large volumes, the active nodes oscillated with a short period (2.5 min) for the duration of the experiment (regime III). However, at intermediate volumes, the gel demonstrated “biperiod” behavior in which short-period (2.5-min) and long-period (10–40-min) oscillations were sustained throughout the experiment (regime II, light gray). The specimens used to create Figure 2 were square and had a range of areas ($0.05\text{--}1.5\text{ mm}^2$) and three different thicknesses (150, 250, and 400 μm). However, all single-to-biperiod transitions collapse onto one curve with respect to volume, indicating that thickness-to-area ratio is not a significant factor. An increase in period length with decreasing specimen volume was previously reported for a PNIPAM BZ gel, but biperiod behavior was not observed.¹¹ Neither the increase in period length nor the existence of two periods have been predicted with current computational models of the BZ system. Accurately modeling the BZ reaction kinetics at small length scales is challenging because intermediate reaction steps, not included in the model, become more significant in this limit. Reaction intermediates in these small volumes might also be responsible for the atypical stability of the metal catalyst in the Ru^{3+} state. In addition, a small number of specimens at low volumes did not oscillate ($n = 5, \leq 0.038\text{ mm}^3$), highlighting the design challenges at lower volumes. To avoid these variations in period behavior, active gel volumes for the following synchronization experiments were taken to be greater than 0.1 mm^3 , where only the short period occurs, and were consistent across samples ($2.5\text{ min} \pm 15\text{ s}$).

2.3. Embedding Increases Likelihood of Node-Pair Synchronization. In the context of BZ gels, synchronization is a sustained series of oscillations of two or more regions of active material with a common period and a constant phase difference. In this study, a “sustained series” means 30 or more continuous oscillations occurring any time after the initial transients ($t > 100\text{ min}$). Pairs of square nodes of active gelatin

were separated by an interspace distance, L , that was normalized to the characteristic length of the BZ system, $L_0 = 30\text{ }\mu\text{m}$ (see the Experimental Section). The average period of oxidation across all specimens was $2.6\text{ min} \pm 23\text{ s}$ for nonembedded nodes and $2.0\text{ min} \pm 46\text{ s}$ for embedded nodes.

Embedment increased the probability of node synchronization for interspace distances of $L/L_0 \leq 15$ (see Figure 3). For

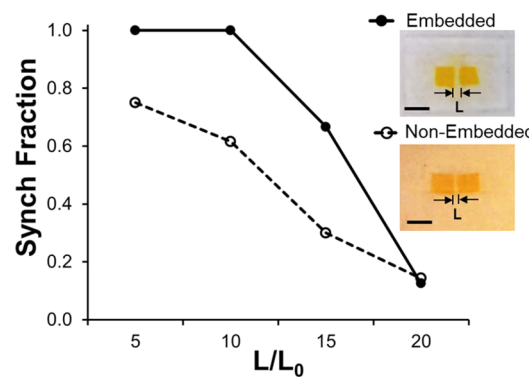


Figure 3. Decrease in synchronization with increasing distance between nodes. Line graph of the fraction of node pairs that synchronized under embedded and nonembedded conditions versus the normalized interspace distance, L/L_0 . Minimum of five node pairs evaluated for each L/L_0 bin and embedment condition. Inset: Images of embedded and nonembedded node pairs. Scale bars = 1 mm, $L_0 = 30\text{ }\mu\text{m}$.

$L/L_0 \leq 10$, all of the embedded node pairs tested experienced a region of synchronization (25 of 25 pairs). The synchrony of nonembedded pairs also decreased with increasing interspace distance, and node pairs were less likely to synchronize than embedded pairs even in the $L/L_0 \leq 10$ range. Above $L/L_0 = 10$, the fraction of synchronized nodes decreased to 0.67 and 0.3 in the $L/L_0 = 15$ bin for embedded and nonembedded pairs, respectively. The synchronization fractions of embedded and nonembedded pairs at $L/L_0 = 20$ (0.13 vs 0.14) were statistically the same, which indicates that embedment can only partially compensate for reduced node proximity.

The increase in synchronization probability and extended synchronization distance with embedment at first appears counterintuitive. The chemical communication of the BZ system is fundamentally dependent on the diffusion of reactants between nodes, which is frustrated by the embedding matrix. Therefore, embedment must provide a compensatory benefit. One possibility is that a slight retardation of diffusion heightens the local accumulation of reactant intermediates. This would increase the sensitivity of the nodes to incoming reactants from neighbors, as the nodes would more readily be at the oxidation threshold. The small decrease in average period between embedded and nonembedded node pairs supports this hypothesis (2.6 vs 2.0 min). The lack of 100% synchronization in nonembedded gels at short interspace distances is also consistent with this explanation. Mechanical communication transferred through the embedding matrix might also enhance the synchronization performance. Smith et al. determined that the strain field of an embedded active node (1.5% strain at source) decays to zero within approximately $300\text{ }\mu\text{m}$.¹⁶ This distance corresponds to $L/L_0 = 10$ in our material system, beyond which the synchronization percentage decreased and synchronized pairs became increasingly antiphase. Hence, it is likely that, within $L/L_0 = 10$, the neighboring nodes detect each

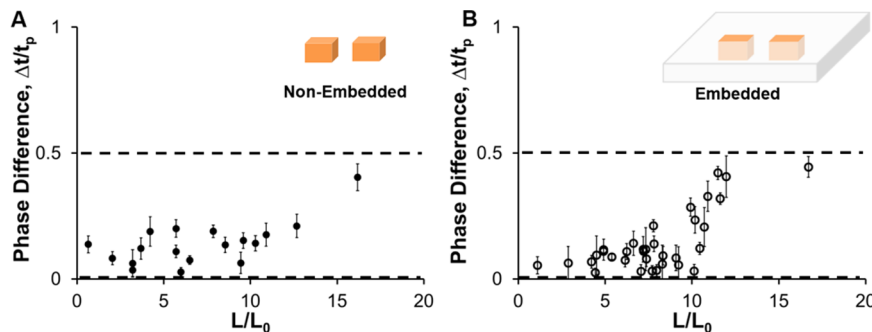


Figure 4. Loss of in-phase synchrony with increasing interspace distance. Plot of phase difference versus interspace distance for (A) nonembedded and (B) embedded node pairs. Each point represents the mean \pm standard deviation of phase difference averaged over ≥ 30 oscillations.

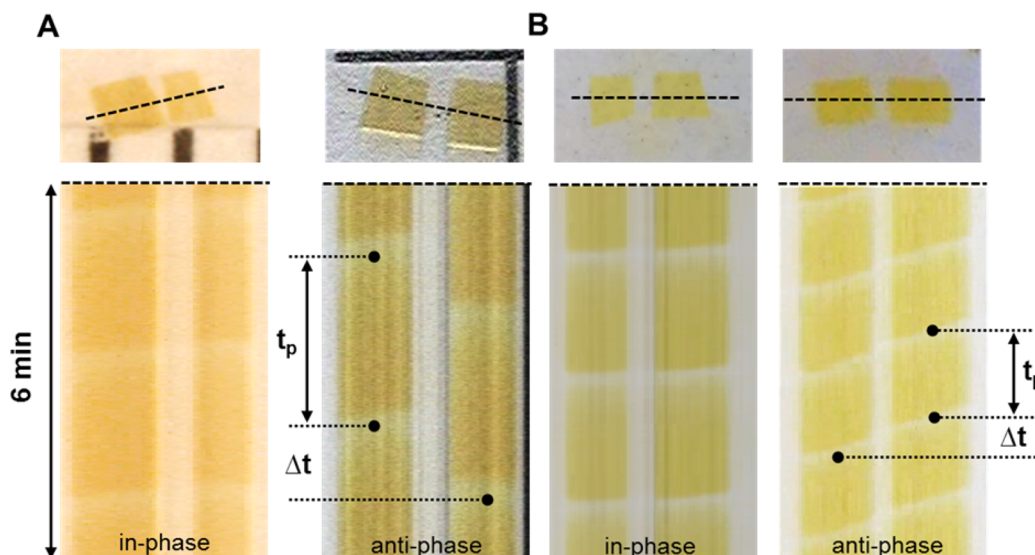


Figure 5. In-phase and near-antiphase synchronization behavior in (A) nonembedded and (B) embedded node pairs. Time along the vertical axis and position along horizontal axis. Total time in all panels is 6 min. Period and phase difference highlighted in antiphase gels. Dark yellow, Ru^{2+} ; translucent/light yellow, Ru^{3+} .

other by the physical displacement of the gelatin network, underlining the importance of mechanical communication.

2.4. In-Phase-to-Antiphase Transition with Increasing Interspace Distance. Synchronized node pairs can oscillate simultaneously (in-phase), a half-period apart (antiphase), or somewhere in between. The time difference between the oxidation waves is known as the phase difference for the two oscillators. The phase difference was normalized by the period of the synchronized oscillations (see the Experimental Section, Figure 7 inset). In both the embedded and nonembedded cases, the phase difference transitioned from near-in-phase ($\Delta t/t_p \approx 0$) to near-antiphase ($\Delta t/t_p \approx 0.5$) with increasing interspace distance (Figure 4). This is the first experimental report of antiphase synchronization in a composite BZ gel. The time-lapse line plots of Ru oxidation and reduction are shown in Figure 5, with extended time plots and return maps provided in Figures S3 and S4 (Supporting Information). The near-antiphase synchronization of the embedded node pair shown in Figure 5B appears to be trigger-induced, meaning that the oxidation wave travels across the node pair. By comparison, the nonembedded antiphase node pair shown in Figure 5A involves isolated initiations in each node. The phase-difference calculation used in this study did not distinguish between these types of oxidation behavior. The transition occurred at $L/L_0 \approx 10$, which is also the interspace distance where the fraction

of synchronized pairs began to significantly decrease. The lower density of data points after $L/L_0 \approx 10$ is a consequence of the reduced number of synchronized node pairs in this range. The transition region for embedded gels might have occurred at interspace distances less than $L/L_0 = 10$; however, the transition for nonembedded gels definitely began at interspacings greater than this critical length.

The transition from in-phase to antiphase synchronization qualitatively agrees with computational predictions for disk-shaped PNIPAM BZ gels separated by PAM spacers.¹⁵ In the study, the critical interspace distances for 100% synchronization (230 μm , $L/L_0 \approx 6.7$) and 0% synchronization (420 μm , $L/L_0 \approx 12.4$) were experimentally determined, but the experimental data for the transition from in-phase to antiphase were not presented. The requisite number of oscillations for synchrony was also not reported. However, the computational results of the study were more complete and evaluated the phase transition with a robust criterion for synchronization of 25–30 cycles. The model predicted a transition from in-phase to antiphase synchronization between $L/L_0 = 2$ and $L/L_0 = 4$. The critical transition point in the model is dependent on the stoichiometric conversion factor, f , of oxidizable agents to bromide by malonic acid. The model predicts that higher conversion factors maintain in-phase synchronization at larger interspace distances, suggesting that a more efficient reaction

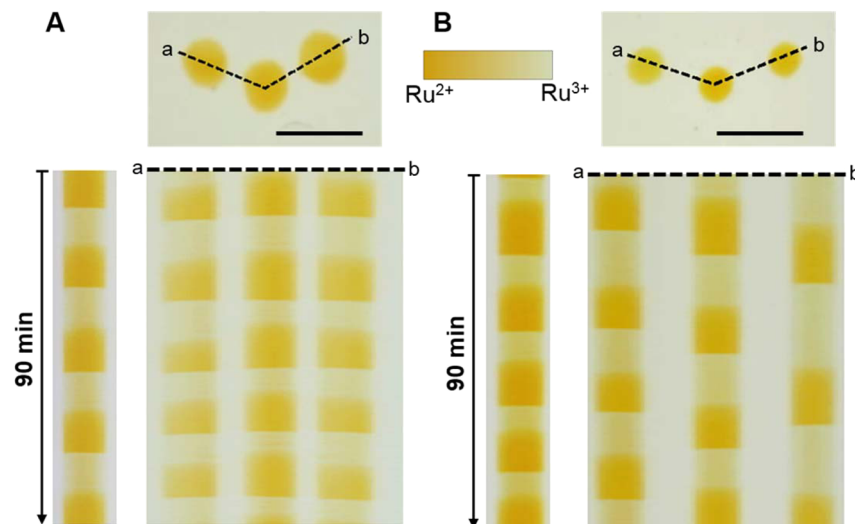


Figure 6. Pair-wise synchronization criteria confirmed in multinode grids: (A) Triad of BZ nodes with $L/L_0 \approx 7$ oscillate in-phase. (B) Triad of BZ nodes with $L/L_0 \approx 15$ oscillate with near-antiphase synchrony and eventually discontinue synchronization. Leftmost column shows the oscillation of a single embedded node that serves as a control. Dark yellow, Ru²⁺; translucent/light yellow, Ru³⁺; clear, inactive gelatin. Scale bars = 1 mm. Note that the period of oscillation is longer in the printed system than in the film stacking system likely because of differences in the through-thickness profile.

can chemically communicate over a greater distance. Our gelatin-based system transitioned from near-in-phase to antiphase synchronization at $L/L_0 \approx 10$ for both the embedded and nonembedded systems. Several factors might contribute to this difference. First, cube-shaped node pairs share a parallel edge and likely a higher interaction strength than disk-shaped pairs. This geometric difference would shift the phase transition of disk-shaped nodes to a lower L/L_0 value. Second, this critical transition distance might be slightly inflated as a result of the underestimation of L_0 . L_0 was calculated using kinetic constants at 20 °C,¹⁸ whereas our BZ reactions were performed at 22–24 °C. Last, the difference in critical transition between PNIPAM/PAM¹⁵ and our gelatin system might result from differences in polymer/BZ solution interaction effects. PNIPAM is electrically neutral, whereas gelatin is a polyampholyte. Solution/polymer interactions of this type are difficult to directly measure and/or model, but could possibly be studied by evaluating the phase-difference transition of synchronized node pairs as a function of polymer concentration and side-chain complexity.

2.5. Demonstration of Synchrony in Multinode Grid. At this point, the results demonstrate that (1) embedment promotes synchronization and (2) interspace distance is the primary regulator of the phase difference of synchronization. To demonstrate the utility of the design criteria, arrays of node triads were printed with in-phase and antiphase interspace distances (see Figure 6). Videos of multinode grids are included in the Supporting Information (Videos V1 and V2).

As seen in Figure 6A, three 500-μm-diameter nodes of active gelatin were printed with interspace distances of $L/L_0 = 8.1$ and 6.8, both within the range of 100% synchronization probability. A single embedded active node was also printed at a distance of $L/L_0 \approx 100$ from the triad as a control (leftmost strip in Figure 6A,B). All three nodes in the triad oxidized together in phase, as indicated by the in-unison transition from dark yellow to clear. Conversely, the active nodes in triads with interspace distances of $L/L_0 = 15.0$ and 15.2 in Figure 6B are not in phase. Instead, the three nodes oscillate at near-antiphase for a few cycles and at later times oscillate with no synchrony at all. Both triad

results agree with the pair data from Figure 4B, suggesting that pairwise synchronization results can effectively inform the construction of larger node systems.

Note that we did observe a slight difference in frequency between the triad and the control, which is likely an effect of multinode interaction. Specifically, the in-phase triad oscillated at a slightly higher frequency than the control, whereas the antiphase triad oscillated at a slightly lower frequency. Further study of triad spacing and arrangement is necessary to fully understand this effect.

3. CONCLUSIONS

Criteria for synchronization behavior of interacting nodes of BZ hydrogels is an essential building block for the effective design of BZ communication networks and devices. The results of this study are consistent with previous modeling predictions of an in-phase-to-antiphase transition of synchronization^{15,17} and with previous experimental results that showed interspace distance between regions of active gel to be a key driver of BZ gel synchronization.^{10,15,16} This study extends these results by developing fabrication techniques for composite BZ thermogels, evaluating synchrony in fully embedded thermogels, demonstrating that embedment increases the likelihood of synchronization, and experimentally confirming that antiphase synchronization occurs at larger interspace distances.

Spatial patterning techniques for self-oscillating BZ hydrogels are dependent on each material system. PNIPAM, the original⁸ and predominant polymer used in BZ gels, requires a cross-link initiator to create its gel-like properties. Maintaining precise boundaries between the active and inactive polymer regions during this cross-linking step is challenging. Other BZ polymers and copolymers that require a chemical cross-linking step, such as PAM,^{11,12} acrylamide-2-methylpropane sulfonic acid (AMPS),¹⁹ and acrylic acid (AAc),²⁰ have the same issue. One solution is to immobilize the Ru catalyst in the polymer after cross-linking through postfunctionalized printing.^{21,22} With this technique, patterning can be automated and have sub-25-μm resolution depending on printer, gel thickness, and

diffusion behavior of the catalyst solvent. Alternatively, BZ gels can be manually arranged after cross-linking using inactive polymer spacers.¹⁵ However, in this setup, the interfaces between the active and inactive polymers exhibit no chain entanglement or chemical cross-links, greatly reducing the mechanical communication possible through swelling. In contrast, BZ thermogels, such as the gelatin used in this study and others,^{16,23} solidify through chain entanglement when cooled through a transition temperature, allowing more robust active and inactive interfaces. The thermogel properties of gelatin are conducive for extrusion-based printing techniques, as the gelation temperature allows the printed structure to hold its shape throughout the printing process. Commercial inkjet printers can dispense ultralow volumes of material ($\sim 10\text{--}100\text{ }\mu\text{L}$), which enables patterning of high resolution structures.²⁴ However, because of the variability in period behavior at low gel volumes ($<0.04\text{ mm}^3$ or $4000\text{ }\mu\text{L}$), BZ devices should be fabricated at a micron-to-millimeter length scale to ensure predictable behavior. Synthetic thermogelling polymers, such as *N*-acryloyl glycaminide,²⁵ are advantageous candidates for future study as composite BZ gels, as they are more chemically homogeneous than protein-based polymers and allow more strategies for tuning amine groups for catalyst immobilization.

The synchronization results of this study confirm that mechanical embedment is advantageous for active-node synchrony and should be considered a prerequisite for the design of autonomous BZ devices. Embedment improved the likelihood of synchrony (Figure 3), and embedded node pairs generated a more distinct transition with interspace distance from in-phase to antiphase synchronization (Figure 4B). Secondary effects, such as the increase in oxidation frequency due to mechanical coupling predicted by Yashin and Balazs¹⁷ were difficult to confirm in our model system. Reasons for this difficulty include differences in the swelling performance of our gels (1–2%) versus the model (30%) and the magnitude of the predicted frequency increase (5–10%) being within the experimental variability. Although additional experiments are needed to fully distinguish the chemical and mechanical contributions to the frequency shifts, the overall stabilization effect of mechanical coupling motivates the design of fully embedded BZ devices.

As design patterns become larger and more complex, additional tests will be needed to identify coupling effects not possible in a node-pair system. The boundary-condition effects of embedded versus nonembedded surfaces will be important to investigate. Our study focused on a grid of active nodes of uniform shape and size; however, shapes with nonunity aspect ratios might behave differently when embedded. Additional studies are needed to incorporate more active-gel geometries and their coupling effects into BZ design tools. Together, the design criteria for synchronization and 3D printing techniques for multinode grids provide a complementary initial basis of tools for developing BZ devices.

4. EXPERIMENTAL SECTION

4.1. Synthesis of Ru Gelatin. All specimens consisted of 10% gelatin type A (~ 300 bloom) acquired from Sigma-Aldrich. Samples of plain gelatin (without Ru) were fabricated using deionized (DI) water in a 2 g/20 mL ratio. Ru-immobilized gelatin (active gelatin) was fabricated at the same ratio with 0.1 M sodium phosphate buffer (SPB) at pH 7.4. Ru immobilization was performed by *N*-hydroxysuccinimide ester

reaction chemistry as previously reported.²² Briefly, bis(2,2'-bipyridine)-4'-methyl-4-carboxybipyridine-ruthenium *N*-succinimidyl ester-bis(hexafluorophosphate) (Sigma-Aldrich 96631) is added in a ratio of 4.1 mg/250 mg 10% SPB gelatin in 1-mg increments while being heated at 42–46 °C for 2–4 h. Small amounts of dimethylformamide (DMF) ($\sim 2\text{--}8\text{ }\mu\text{L}/\text{mg}$ of Ru) can be added to assist dissolution. After patterning, the composite BZ gels were placed in 5 mM glutaraldehyde (Sigma-Aldrich 5882) for 24 h at 4 °C to chemically cross-link the gel. The average Ru concentration across nine batches was $0.7 \pm 0.2\text{ mM}$ in swollen gels, as measured using UV-vis spectroscopy (additional details in the Supporting Information).

4.2. BZ Reaction Conditions. All specimens were placed in solutions with initial BZ reactant concentrations of 0.7 M nitric acid, 0.08 M sodium bromate, and 0.04 M malonic acid (MA). The period of oxidation of the Ru catalyst is largely regulated by reaction temperature and the initial concentrations of these three reactants. The empirical relations between period and reactant concentrations have been determined for PNIPAM,¹⁰ PAM,²¹ and gelatin²³ BZ systems. Of the three reactants, period length is most sensitive to the MA concentration, where period length is inversely related to MA concentration.^{13,23} In this study, MA was tuned for a target period of 2.5 min to observe a large number of cycles for more robust evaluation of node-pair synchronization. The initial reactant concentrations also largely determine the characteristic length of the BZ system, L_0 , as previously defined in ref 23 and as implemented for a gelatin BZ system in reference 16. In, brief

$$L_0 = (D_u T_0)^{1/2} \quad (1)$$

where $D_u \approx 2 \times 10^{-5}\text{ cm}^2\text{ s}^{-1}$ is the diffusion coefficient of a dissolved reactant in water and $T_0 = (k_3[\text{H}][\text{A}])^{-1}$ is the characteristic time of the autocatalytic reaction in the BZ system. The autocatalytic rate is assumed to be $k_3 = 42\text{ M}^{-2}$ as measured in BZ solution at 20 °C,^{18,26} where [H] corresponds to the hydrogen-ion molar concentration (0.7 M) and [A] corresponds to the sodium bromate (0.08 M) molar concentration. Together, this results in a characteristic length of $L_0 = 30\text{ }\mu\text{m}$, which was used to normalize the interspace distance for synchronization.

4.3. Synchrony Analysis from Images. Hydrated composite specimens were placed in 5 mL of unstirred reactants for the duration of the experiment. Initial oxidation of the Ru catalyst occurred within 5 min for isolated nodes and within 15 min for embedded node pairs. Approximately 10–15% area shrinkage occurred within the first 20 min in BZ solution, as observed in a previous BZ gelatin system,¹⁶ which is a typical response of a hydrogel to a high-ionic-strength solution.²⁷ The BZ reaction was performed at room temperature (22–24 °C). Time-lapse video was collected using a DinoCam at a rate of one image per second for 5 h. Minimal degradation of the gel was observed during this period; however, after 24 h, the gel was effectively dissolved in the BZ solution. Postprocessing of the video data was semiautomated using custom Matlab scripts. First, the periodic oxidation and reduction of the Ru catalyst were measured in the center of each BZ node, using the signal intensity of the blue channel. The period of the oscillation was measured as the distance between oxidation peaks. Oxidation profiles and period plots for single-node oscillations are shown in Figure S2 (Supporting Information). To avoid transient effects of the BZ reaction,

only data after 100 min were used for further analysis. Phase difference was defined as the time between oxidation peaks of node pairs, Δt , divided by the period, t_p , of the node with the leading oscillation (Figure 7, inset). A node pair was considered

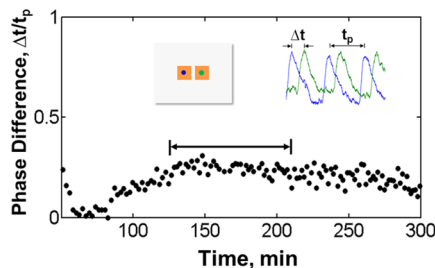


Figure 7. Quantification method of BZ gel synchronization. Plot of phase difference, $\Delta t/t_p$, versus reaction time. In-phase, $\Delta t/t_p = 0$; antiphase, $\Delta t/t_p = 0.5$. All data for $t < 100$ min were considered to reflect transient behavior. Arrow indicates a region of ≥ 30 consecutive cycles with near-constant phase ($\Delta t/t_p \approx 0.25$). Insets: Schematic of an embedded node pair with colored dots indicating locations of signal intensity reading. Example signal intensities of a BZ node pair with definition of phase difference at upper right.

synchronized if it exhibited an approximately constant phase segment of 30 or more consecutive cycles at any time between 100 and 300 min (Figure 7, arrow). This synchronization criterion extends the current number of experimentally reported synchronized oscillations (< 10)¹⁶ and is in agreement with the quantity used in computational studies (25–30).¹⁵ For each synchronized node pair, the phase difference is presented as the mean \pm standard deviation across the synchronized cycles (Figure 4). The synchronization fraction is defined as

$$\text{synchronization fraction} = \frac{\text{no. of node pairs synchronized}}{\text{total no. of node pairs tested}} \quad (2)$$

and was calculated for each interspace distance grouping. A minimum of five pairs were tested for each interspace distance bin and embedment condition.

■ ASSOCIATED CONTENT

S Supporting Information

Additional experimental details and supporting results. This material is available free of charge via the Internet at <http://pubs.acs.org>.

■ AUTHOR INFORMATION

Corresponding Author

*E-mail: richard.vaia@us.af.mil.

Notes

The authors declare no competing financial interest.

■ ACKNOWLEDGMENTS

The authors thank Anna Balazs, Victor Yashin, and Olga Kuksenok for their helpful discussions and feedback regarding this study. The authors also thank Art Safriet for the design and fabrication of the gelatin cutting jig. Funding from Air Force Office of Scientific Research and the Air Force Research Laboratory's Materials and Manufacturing Directorate is gratefully acknowledged.

■ REFERENCES

- Gerisch, G.; Hess, B. Cyclic-AMP-Controlled Oscillations in Suspended Dictyostelium Cells: Their Relation to Morphogenetic Cell Interactions. *Proc. Natl. Acad. Sci. U.S.A.* **1974**, *71*, 2118–2122.
- Mirocco, R. E.; Strogatz, S. H. Synchronization of Pulse-Coupled Biological Oscillators. *J. Appl. Math.* **1990**, *50*, 1645–1662.
- Parrish, J. K.; Edelstein-Keshet, L. Complexity, Pattern, and Evolutionary Trade-Offs in Animal Aggregation. *Science* **1999**, *284*, 99–101.
- Smith, H. M. Synchronous Flashing of Fireflies. *Science* **1935**, *82*, 151–152.
- Kiss, I. Z.; Zhai, Y.; Hudson, J. L. Emerging Coherence in a Population of Chemical Oscillators. *Science* **2002**, *296*, 1676–1678.
- Taylor, A. F.; Tinsley, M. R.; Wang, F.; Huang, Z.; Showalter, K. Dynamical Quorum Sensing and Synchronization in Large Populations of Chemical Oscillators. *Science* **2009**, *323*, 614–617.
- Epstein, I. R.; Showalter, K. Nonlinear Chemical Dynamics: Oscillations, Patterns, and Chaos. *J. Phys. Chem.* **1996**, *100*, 13132–13147.
- Yoshida, R.; Takahashi, T.; Yamaguchi, T.; Ichijo, H. Self-Oscillating Gel. *J. Am. Chem. Soc.* **1996**, *118*, 5134–5135.
- Maeda, S.; Hara, Y.; Yoshida, R.; Hashimoto, S. Peristaltic Motion of Polymer Gels. *Angew. Chem.* **2008**, *120*, 6792–6795.
- Yoshida, R.; Tanaka, M.; Onodera, S.; Yamaguchi, T.; Kokufuta, E. In-Phase Synchronization of Chemical and Mechanical Oscillations in Self-Oscillating Gels. *J. Phys. Chem. A* **2000**, *104*, 7549–7555.
- Chen, I. C.; Kuksenok, O.; Yashin, V. V.; Moslin, R. M.; Balazs, A. C.; Van Vliet, K. J. Shape- and Size-Dependent Patterns in Self-Oscillating Polymer Gels. *Soft Matter* **2011**, *7*, 3141–3146.
- Yuan, P.; Kuksenok, O.; Gross, D. E.; Balazs, A. C.; Moore, J. S.; Nuzzo, R. G. UV Patternable Thin Film Chemistry for Shape and Functionally Versatile Self-Oscillating Gels. *Soft Matter* **2013**, *9*, 1231–1243.
- Chen, I. C.; Kuksenok, O.; Yashin, V. V.; Balazs, A. C.; Van Vliet, K. J. Mechanical Resuscitation of Chemical Oscillations in Belousov–Zhabotinsky Gels. *Adv. Funct. Mater.* **2012**, *22*, 2535–2541.
- Tateyama, S.; Shibata, Y.; Yoshida, R. Direction Control of Chemical Wave Propagation in Self-Oscillating Gel Array. *J. Phys. Chem. B* **2008**, *112*, 1777–1782.
- Yashin, V. V.; Suzuki, S.; Yoshida, R.; Balazs, A. C. Controlling the Dynamic Behavior of Heterogeneous Self-Oscillating Gels. *J. Mater. Chem.* **2012**, *22*, 13625–13636.
- Smith, M. L.; Slone, C.; Heitfeld, K.; Vaia, R. A. Designed Autonomic Motion in Heterogeneous Belousov–Zhabotinsky (BZ)-Gelatin Composites by Synchronicity. *Adv. Funct. Mater.* **2013**, *23*, 2835–2842.
- Yashin, V. V.; Balazs, A. C. Chemomechanical Synchronization in Heterogeneous Self-Oscillating Gels. *Phys. Rev. E* **2008**, *77*, 046210.
- Field, R. J.; Foersterling, H. D. On the Oxybromine Chemistry Rate Constants with Cerium Ions in the Field–Körös–Noyes Mechanism of the Belousov–Zhabotinskii Reaction: The Equilibrium $\text{HBrO}_2 + \text{BrO}_3^- + \text{H}^+ \rightleftharpoons 2\text{BrO}_2^\bullet + \text{H}_2\text{O}$. *J. Phys. Chem.* **1986**, *90*, 5400–5407.
- Hara, Y.; Yoshida, R. Control of Oscillating Behavior for the Self-Oscillating Polymer with pH-Control Site. *Langmuir* **2005**, *21*, 9773–9776.
- Ito, Y.; Nogawa, M.; Yoshida, R. Temperature Control of the Belousov–Zhabotinsky Reaction Using a Thermoresponsive Polymer. *Langmuir* **2003**, *19*, 9577–9579.
- Kramb, R. C.; Buskohl, P. R.; Slone, C.; Smith, M. L.; Vaia, R. A. Autonomic Composite Hydrogels by Reactive Printing: Materials and Oscillatory Response. *Soft Matter* **2014**, *10*, 1329–36.
- Smith, M. L.; Heitfeld, K.; Slone, C.; Vaia, R. A. Autonomic Hydrogels through Postfunctionalization of Gelatin. *Chem. Mater.* **2012**, *24*, 3074–3080.
- Smith, M. L.; Heitfeld, K.; Tchoul, M.; Vaia, R. A. Chemical Wave Characterization of Self-Oscillating Gelatin and Polyacrylamide Gels. In *SPIE Smart Structures and Materials + Nondestructive*

Evaluation and Health Monitoring; International Society for Optics and Photonics: Bellingham, WA, 2011; pp 79750A-1–79750A-8.

(24) Chouiki, M.; Schoeftner, R. Inkjet Printing of Inorganic Sol–Gel Ink and Control of the Geometrical Characteristics. *J. Sol-Gel Sci. Technol.* **2011**, *58*, 91–95.

(25) Glatzel, S.; Badi, N.; Päch, M.; Laschewsky, A.; Lutz, J.-F. Well-Defined Synthetic Polymers with a Protein-Like Gelation Behavior in Water. *Chem. Commun.* **2010**, *46*, 4517–4519.

(26) Amemiya, T.; Ohmori, T.; Yamaguchi, T. An Oregonator-Class Model for Photoinduced Behavior in the Ru(bpy)₃²⁺-Catalyzed Belousov–Zhabotinsky Reaction. *J. Phys. Chem. A* **2000**, *104*, 336–344.

(27) Okay, O. General Properties of Hydrogels. In *Hydrogel Sensors and Actuators*; Springer: Berlin, 2010; pp 1–14.